# Understanding the Mechanism of Triplet-Triplet Energy Transfer in the Photocatalytic [2+2] Cycloaddition: Insights from Quantum Chemical Modeling

Eunji Lee[a,b], Hyejin Moon[a,b], Jiyong Park,[b,a*] and Mu-Hyun Baik[b,a*]

[a]Department of Chemistry, Korea Advanced Institute of Science and Technology (KAIST), Daejeon, 34141, Republic of Korea

[b]Center for Catalytic Hydrocarbon Functionalizations, Institute for Basic Science (IBS), Daejeon, 34141, Republic of Korea

**ABSTRACT:** This study investigates the mechanism of the [2+2] photocycloaddition reaction of 3-(but-3-enyl)oxyquinolone using a chiral xanthone-containing triplet sensitizer. Quantum chemical computer models were utilized to examine the substrate-catalyst encounter complex structures, which were classified into *syn*- and *anti*-adducts. The photoactivation steps of the substrate were analyzed based on the Marcus equation of electron transfer, including intersystem crossings (ISC) and outer sphere triplet-triplet energy transfer (TTEnT). Our results show that the calculated rates of ISC are comparable for the two adducts, while the computed rates of TTEnT differ between them due to the orbital overlap between the donor and acceptor sites. After the TTEnT, a stereospecific cyclization occurs, completing the catalytic cycle. We propose a novel strategy to improve stereoselectivity by exploiting the intrinsic difference in TTEnT rates between the two encounter complex isomers.

# Introduction

The photoactivated [2+2] cycloaddition of enones and alkenes provides a valuable route to cyclobutanes, circumventing the constraints posed by the orbital symmetry-forbidden nature of thermal [2+2] reactions in the ground state.[1] Unfortunately, traditional approaches relying on high-powered UV-light sources typically suffer from low degrees of stereo- and regioselectivity, as well as undesirable side reactions, which limits their practical utility. Recently, the use of triplet photosensitizers has emerged as a promising alternative, offering superior light absorption efficiency and substrate activation by delivering the precise amount of energy needed for activation to the desired substrate. Organic triplet sensitizers incorporating stereospecific hydrogen bonding scaffolds have been developed, achieving remarkable enantioselectivity in [2+2] photocycloadditions.[2–9] Inorganic triplet sensitizers, such as chiral Ir(III) and Ru(II) photocatalysts bearing hydrogen bonding scaffolds, have also been investigated and demonstrated high enantioselectivities.[10–12]

The mechanistic understanding of the [2+2] photocycloadditions of enones and alkenes was pioneered by Corey and De Mayo.[13–15] This mechanism involves the photoexcitation of the enone substrate, followed by intersystem crossing (ISC) to yield a triplet biradical species, which then undergoes a stepwise [2+2] cycloaddition with the ground state alkene substrate.[16–18] In photocatalytic processes, the photoexcitation and rapid ISC within the photocatalyst allow the sensitizer to access the triplet excited state manifold. Subsequently, a triplet-triplet energy transfer (TTEnT) follows that exchanges the triplet character of the sensitizer and the singlet character of the enone substrate. Here, TTEnT is mediated by a two-electron exchange mechanism known as the Dexter process.[19–22] After the TTEnT, the substrate accesses its triplet manifold and undergoes the bond-forming events in a stepwise manner.[23,24]

Previously, we examined the origins of stereoselectivity in intra- and intermolecular [2+2] cycloadditions activated by chiral iridium triplet sensitizers using density functional theory (DFT) calculations.[10,11,25] We also studied the activation barriers and rates of intramolecular [2+2] photocycloadditions assisted by Brønsted acids.[26] The rates of triplet energy transfer between the hydrogen-bonded donor and acceptor moieties, however, have not been fully characterized yet. This is mainly due to experimental and theoretical challenges in precisely quantifying the rates of TTEnT between the photosensitizer and the substrate.

**Scheme 1.** Enantioselective [2+2] cycloaddition reaction of **2** mediated by chiral organic photocatalyst **1**

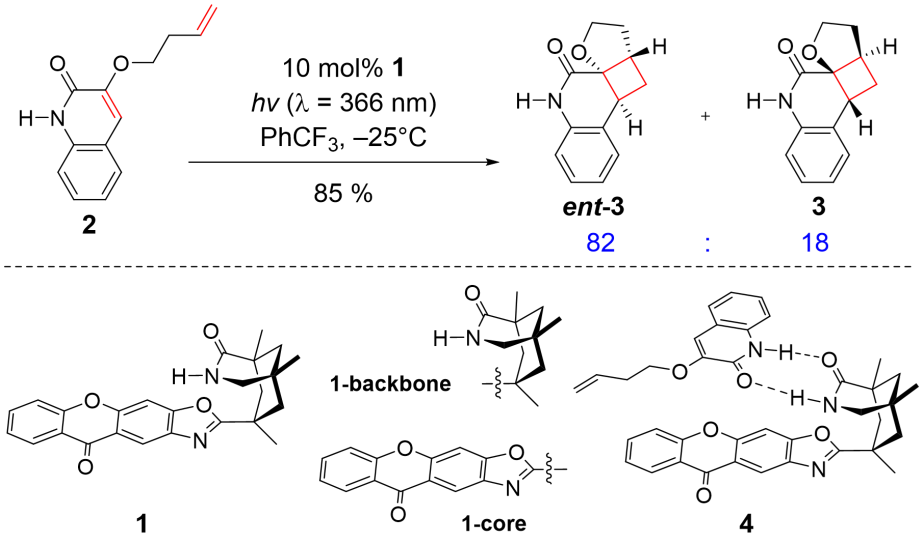


In this study, we investigate the detailed mechanism of the enantioselective intramolecular [2+2] photocycloaddition of an enone substrate **2** using the xanthone containing chiral organic photocatalyst **1**, previously reported by the Bach group (Scheme 1).[4] Photocatalyst **1** consists of an organic photoactive core **1-core** and the lactam backbone **1-backbone** that binds the substrate **2** using two hydrogen bonds to afford the encounter complex **4**. Quantum chemical analysis based on the uncontroversial structure of the donor-acceptor adduct enhances our intuition about how the donor and acceptor couple in the TTEnT process that has been elusive in earlier examples.[27,28] The organic photocatalyst **1** plays three roles: (*i*) as a photosensitizer that absorbs light energy and transfers it to the substrate; (*ii*) as a chiral catalyst that provides a stereospecific environment; (*iii*) as a facilitator of TTEnT that places the donor and acceptor pair in close proximity to ensure proper orbital overlap. Unlike previous computational mechanistic studies based on extensive multireference *ab initio* calculations,[27–29] we apply a simple two-state description of the electronic coupling based on the fragment excitation difference method in combination with time-dependent density functional (TDDFT) calculations, to quantify the rates of TTEnT.[30,31] Lastly, we propose a novel design strategy that utilizes the TTEnT process to induce stereospecific outcomes.

## Results and Discussion

Scheme 2 shows the proposed mechanism for the intramolecular [2+2] cycloaddition reaction mediated by the chiral organic photocatalyst **1**. The reaction begins with the association of **1** and **2** through hydrogen bonding to form the encounter complex **4**. Absorption of light by the photosensitizer **1-core**[2] yields the first singlet excited species **5**,

following Kasha's rule.[32] Subsequently, ISC gives access to the triplet species **6**, which can carry out the TTEnT to activate the substrate and form the triplet adduct **7**, enabling the enantioselective [2+2] cycloaddition to occur. The reaction proceeds via the formation of an intermediate **8**, which undergoes radical recombination to generate the product complex **9**. Finally, the product ***ent*-3** is released and another equivalent of substrate **2** binds to restart the catalytic cycle.

**Scheme 2.** Proposed catalytic cycle of the [2+2] photocycloaddition reaction of **2** starting from the encounter complex **4**

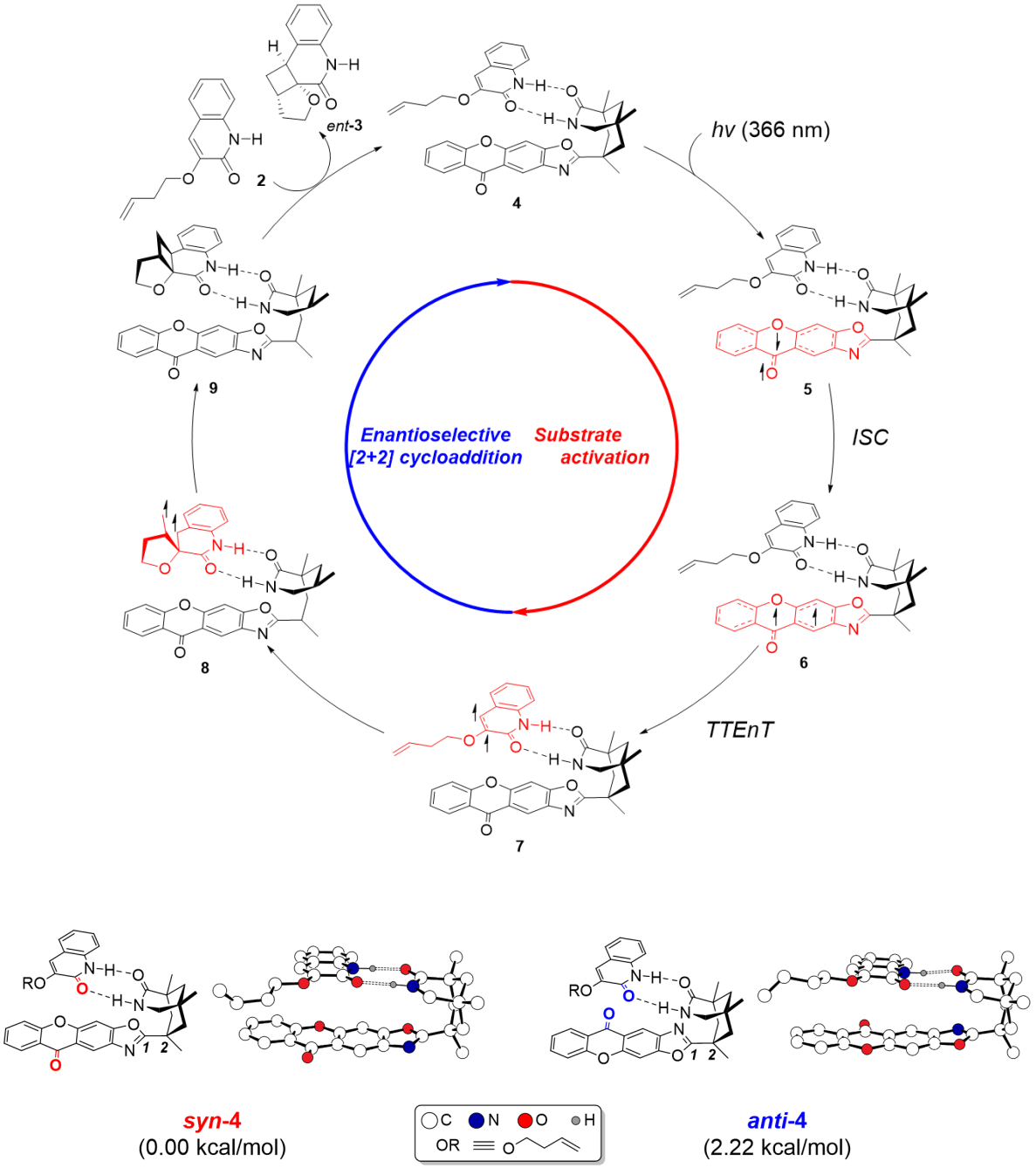

**Figure 1**. Viable structures of catalyst-substrate adducts optimized by DFT calculations. Hydrogens attached to carbons are omitted for clarity.

Viable structures of the catalyst-substrate encounter complex were identified by DFT calculations and are shown in Figure 1. The experimentally observed enantioselectivity originates from the stereo-selective binding of the substrate by a strategically placed hydrogen bond donor/acceptor pair on the chiral catalyst, ensuring that the substrate can only bind in a way that exposes the same molecular face to the photoactive **1-core**, as illustrated for the encounter complex **4** in Scheme 2. Albeit enhancing enantioselectivity, the presence of hydrogen bonding between the substrate and photosensitizer is not a necessary condition for the intermolecular triplet-triplet energy transfer. This is exemplified by photosensitized excited state [2+2] cycloadditions published recently.[33–35] Without the intermolecular hydrogen bondings, however, the observed outcomes are racemic, manifesting the importance of the intermolecular bonding interaction for the stereospecific outcomes. During the stereo-selective [2+2] cycloaddition, the **1-core** sterically protects one of the molecular faces of substrate **2** and forces the intramolecular [2+2] cycloaddition to proceed in a stereoselective fashion. During the exploration of possible structures for this key encounter complex, we realized that the xanthone-containing fragment **1-core** can freely rotate around the C1–C2 single bond that connects it to the **1-backbone** when no substrate is present. As a result, both faces of **1-core** can be exposed to substrate **2**, affording two distinct encounter complexes, labeled as ***syn*-4** and ***anti*-4**. The *syn* and *anti* labels denote the spatial arrangement of the carbonyl group of **1-core** to that of **2**. The Gibbs free energy difference between the lowest energy structures of these two classes of encounter complex is 2.2 kcal/mol, favoring ***syn*-4** with a predicted population ratio of 86:1 under equilibrium conditions at –25 ˚C. This thermodynamic preference for the *syn*-adduct suggests a built-in stereoselectivity for which of the two possible faces of xanthone will be in contact with the substrate. This is an additional stereochemical complexity that has not been appreciated thus far. In this specific case, exploiting this innate stereoselectivity is not possible as both encounter complexes produce the same enantiomer, ***ent*-3**. That is, both ***syn*-4** and ***anti*-4** block the same face of the substrate and the stereoselective [2+2] cycloaddition will proceed in identical ways.

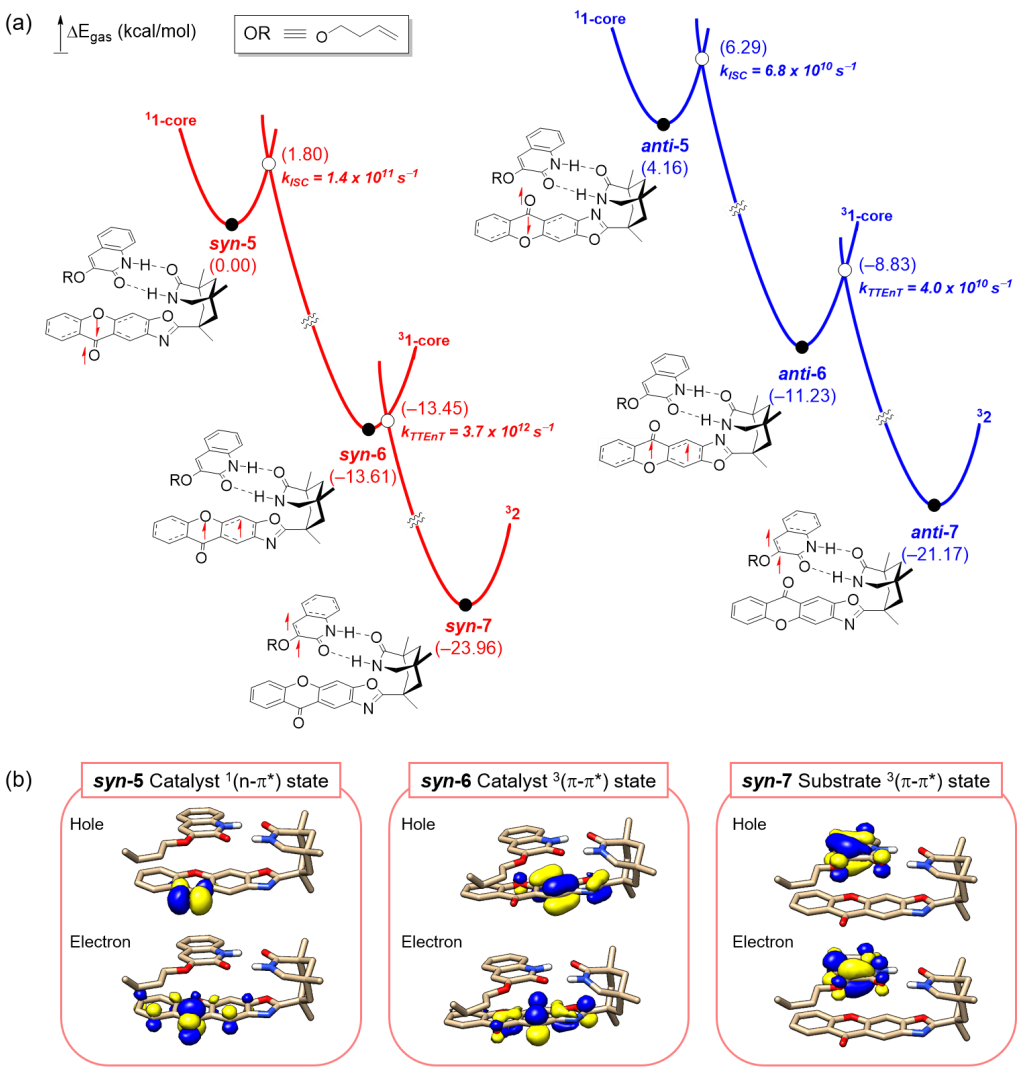


**Figure 2**. (a) Computed energy profile of the ISC and TTEnT steps and (b) The hole and electron pairs of natural transition orbitals of the three excited states.

Figure 2a depicts the energy profiles of the photophysical relaxation process leading to the formation of triplet excited state substrates. To compute the rates of ISC and TTEnT, we employed a combination of Marcus theory of electron transfer and time-dependent density functional theory (TD-DFT) at the TD-CAM-B3LYP-D3/6-31G(d,p) level of the theory. Details of these calculations are provided in the Computational Details section in the supporting information. Upon UV/Vis irradiation, high-energy singlet excited states are initially populated, subsequently relaxing to the first excited singlet state following Kasha's rule.[32] Our geometry optimizations focused on two lowest-energy singlet excited state species, namely ***syn*-5** and ***anti*-5**. The natural transition orbitals of ***syn*-5**, visualized in Figure 2b, reveal that the excited state is reached through an n→π* transition, involving the transfer of an electron from the non-bonding orbital of carbonyl to the π* orbital of **1-core**. Of note, it is important to analyze the decomposition of the natural transition orbital. The ***syn*-5**

consists of both n→π* and π→π* transition characters as shown in Table S1. The mixed transition character leads to a higher SOC value than expected (Table S2).

Moving forward, the intermediates ***syn*-5** and ***anti*-5** undergo ISC, transforming into the triplet species ***syn*-6** and ***anti*-6**, respectively. The calculated ISC rates from ***syn*-5** to ***syn*-6** and ***anti*-5** to ***anti*-6** are 1.4 x $10^{11}$ and 6.8 x $10^{10}$ $s^{-1}$, corresponding to activation barriers of 1.8 and 2.1 kcal/mol, respectively.[36] Thus, the ISC rates are comparable for both the *syn*- and *anti*-isomers, highlighting that the electronic transition occurs within **1-core**, independent of the structural orientation toward the hydrogen-bonded substrate. These computed rates of ISC and the nature of the electronic transition that changes from $^1$(n→π*) to $^3$(π→π*) are in good agreement with previous reports on the photophysical properties of xanthone[37–41] and a recent computational study based on the wavepacket dynamics calculations.[42]

Next, we investigated the rates of TTEnT from ***syn*-6** to ***syn*-7** and from ***anti*-6** to ***anti*-7**. Formally, the TTEnT involves a simultaneous exchange of two electrons, known as the Dexter energy transfer, where proper overlap between the frontier orbitals of the donor-acceptor pair is crucial. We hypothesized that the *syn*- and *anti*-isomers would facilitate the TTEnT at different rates due to different degrees of orbital overlap. Indeed, our calculations indicated that the TTEnT is ~100 times faster in the ***syn*-6** than in the ***anti*-6** isomer: the computed rates of TTEnT are 3.7 x $10^{12}$ and 4.0 x $10^{10}$ $s^{-1}$, corresponding to activation barriers of 0.2 and 2.4 kcal/mol at –25 ˚C , respectively (Figure 2a).[36] Thus, the *syn*-isomer is innately advantageous for TTEnT, and likely responsible for the successful [2+2] photocycloaddition reaction. As mentioned above, both structural isomers produce the same product in this case. The innate facial selectivity, however, is an interesting feature that deserves additional attention in the future for designing other stereoselective versions of this useful reaction.

**Table 1**. Detailed parameters for the computations of $k_{ISC}$ and $k_{TTEnT}$.

| Transition | Rate const. ($s^{-1}$) | $V_{ISC}$ or $V_{TTEnT}$ ($cm^{-1}$) | ΔG (kcal/mol) | λ (kcal/mol) |
|---|---|---|---|---|
| ***syn*-5** $^1$(n-π*)→***syn*-6** $^3$(π-π*) | $k_{ISC} = 1.4 \times 10^{11}$ | 20 | –13.61 | 13.59 |
| ***syn*-6** $^3$(π-π*)→***syn*-7** $^3$(π-π*) | $k_{TTEnT} = 3.7 \times 10^{12}$ | 208 | –10.36 | 17.53 |
| ***anti*-5** $^1$(n-π*)→***anti*-6** $^3$(π-π*) | $k_{ISC} = 6.8 \times 10^{10}$ | 16 | –15.40 | 17.27 |
| ***anti*-6** $^3$(π-π*)→***anti*-7** $^3$(π-π*) | $k_{TTEnT} = 4.0 \times 10^{10}$ | 31 | –9.93 | 19.19 |

$k_{ISC}$, $k_{TTEnT}$ , $V_{ISC}$ , $V_{TTEnT}$, ΔG and λ, denoting ISC rate constant, TTEnT rate constant, spin-orbit coupling constant, TTEnT electronic coupling constant, energetic driving force and reorganization energy respectively

Comparing the three components of TTEnT within the framework of Marcus theory, namely, the electronic coupling ($V_{TTEnT}$), the thermodynamic driving force (ΔG), and the reorganization energy (λ), we found that the electronic coupling contributed the most to the difference in the rates of TTEnT (Table 1). Of note, the $V_{TTEnT}$ is a direct measure of orbital overlap between the initial and the final electronic states of TTEnT in the Marcus equation of energy transfer.[21,43] For the *syn*-adduct, the $V_{TTEnT}$ between the initial and the final states of TTEnT (***syn*-6** and ***syn*-7**) is 208 $cm^{-1}$, which is ~7 times higher than that of *anti*-isomer (31 $cm^{-1}$). The difference in the strengths of electronic coupling accounts for 49-fold higher rate of TTEnT in the *syn*-adduct over the *anti*-counterpart.

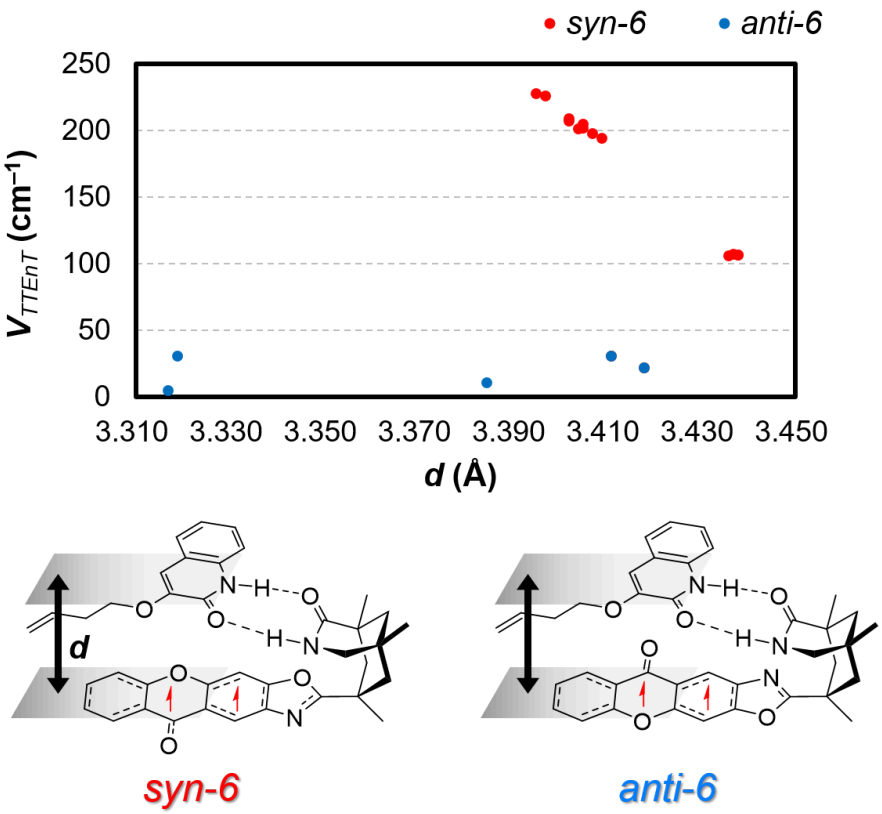


**Figure 3**. Relationship between coupling constant $V_{TTEnT}$ and distance (***d***) between **1-core** and **2**

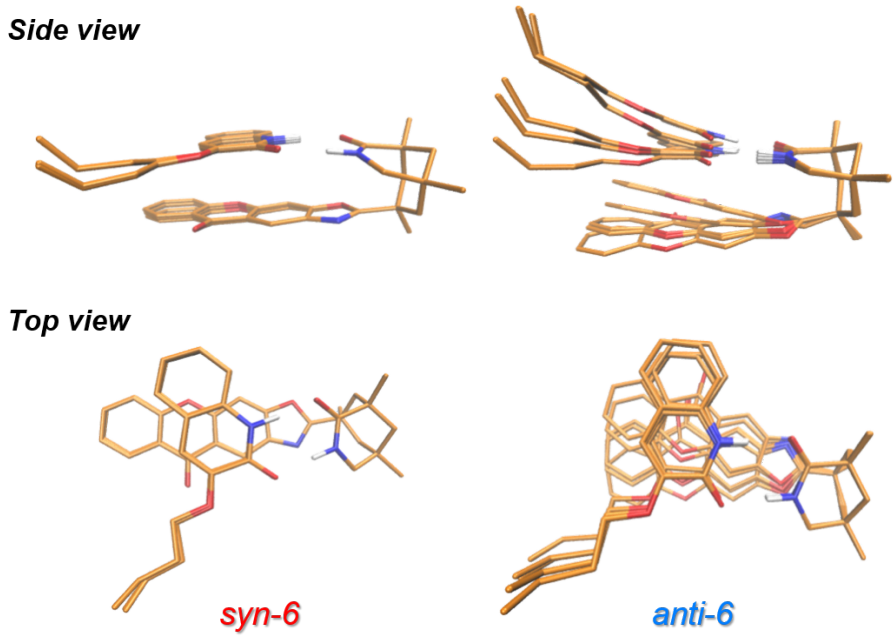


**Figure 4**. Structures of 12 conformers for ***syn*-6** and 5 conformers for ***anti*-6**.

We investigated how the structural differences of the catalyst-substrate encounter complexes influence the $V_{TTEnT}$. Figure 3 shows the distribution of $V_{TTEnT}$ computed from conformers of ***syn*-6** and ***anti*-6**. Previous investigations of intramolecular TTEnT revealed a strong correlation between the electronic coupling strength ($V_{TTEnT}$) and the intermolecular distances (***d***) between the triplet-sensitizer and the acceptor.[44] Prompted by these findings, we computed $V_{TTEnT}$ from a set of *syn*- and *anti*-conformers, varying the distance (***d***) between the triplet donor (**1-core**) and accepter **2**. To identify these conformers, we performed a conformational search, which yielded 12 local minima for ***syn*-6** and 5 for ***anti*-6**. The conformational energies of the identified local minima are comparable to those of the lowest energy structure (Table S3). As the superposition of the 12 *syn*-conformer structures illustrates (Figure 4), the structural difference between them is small with meaningless structural fluctuations in the branched alkene chain being the dominant difference. Thus, all of the optimized *syn*-conformers exhibit nearly identical arrangements between **1-core** and **2**. In contrast, the 5 conformers of ***anti*-6** showed diverse arrangements between **1-core** and **2**. The $V_{TTEnT}$ values for *syn*-conformers ranged from 106 to 228 $cm^{-1}$, where the Boltzmann-weighted average and its standard deviation was 195 ± 26 $cm^{-1}$. On the other hand, the maximum $V_{TTEnT}$ of *anti*-conformers was 31 $cm^{-1}$ and the Boltzmann-weighted average value was 30 ± 1 $cm^{-1}$. Of note, we used the Boltzmann factor of electronic energy as the statistical weight of each conformer (see Supporting Information for details). When compared with the coupling strengths computed from the lowest-in-energy conformers

(Table 1), we concluded that the computations of $V_{TTEnT}$ and the rates of *TTEnT* from the most stable conformers bear statistical significance as well.

Interestingly, the $V_{TTEnT}$ exhibited a linear correlation with the intermolecular distance (***d***) in *syn*–conformers (Figure 3, red). However, such a dependence could not be observed for the *anti*–conformers (Figure 3, blue). These observations suggest that the *syn*-complexes possess a characteristic arrangement between **1-core** and **2**, leading to higher $V_{TTEnT}$ values and showing a linear correlation with the intermolecular distance ***d***.

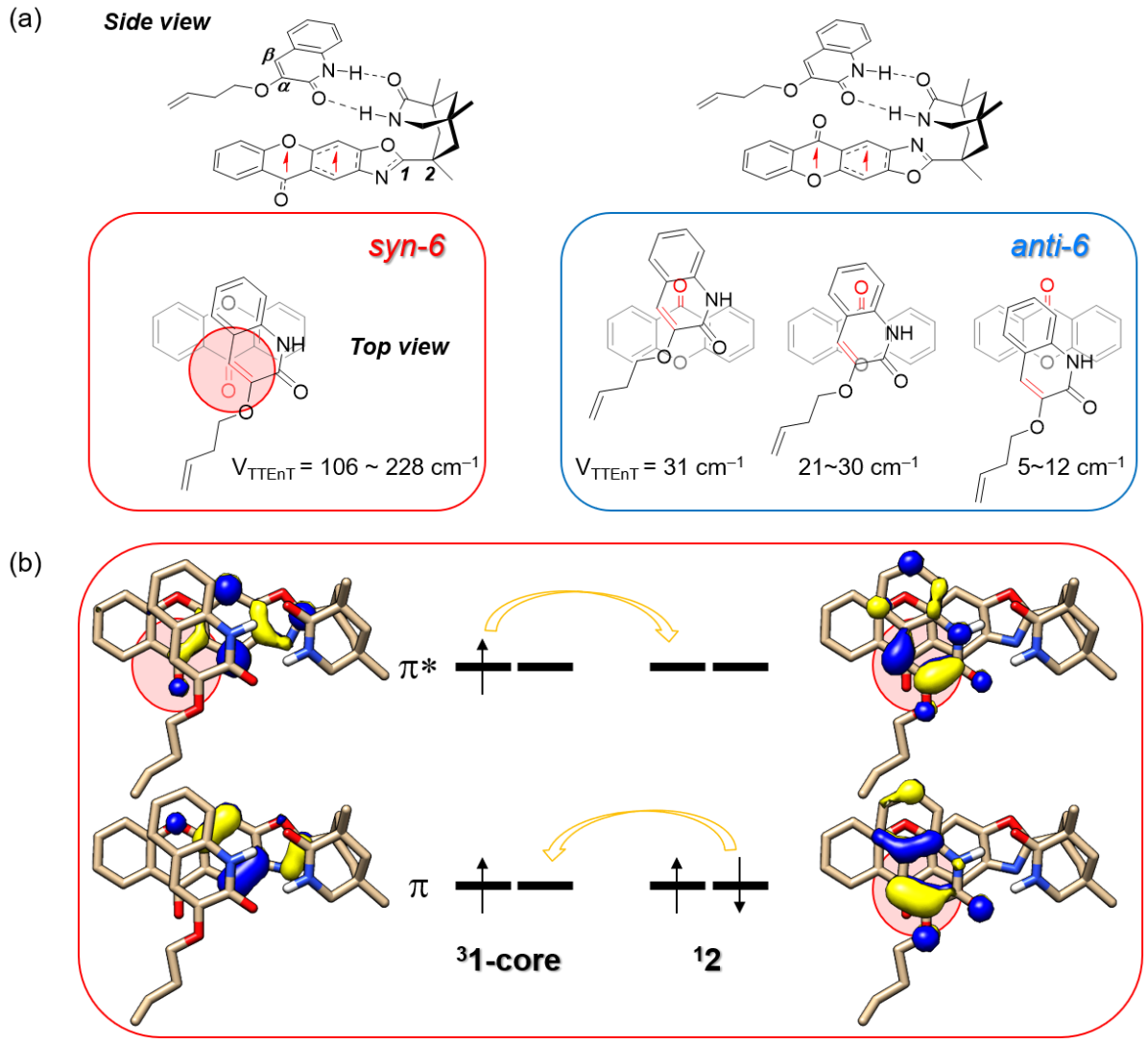


**Figure 5**. (a) Lewis structure illustrations of optimized structures of **6** for *syn* and *anti* compounds shown from side and top views (b) Top view of natural transition orbitals participating in the two-electron transfer process of the ***syn*-6**. The region with strong orbital overlap is highlighted in red circles

The enhanced electronic coupling ($V_{TTEnT}$) in the *syn*-adducts can be attributed to the favorable orbital overlap between the photosensitizer **1-core** and the substrate **2**, which

functions as the triplet energy donor and the acceptor, respectively. The Lewis structures of ***syn*-6** and ***anti*-6** are illustrated in Figure 5a. As detailed in Figure 4, the arrangement of **1-core** and **2** in ***syn*-6** is unique, whereas their arrangement in ***anti*-6** can be classified into three different structure types, none of which offers an ideal donor-acceptor orbital overlap. The natural transition orbitals of ***syn*-6** before and after the TTEnT process are represented in Figure 5b. The TTEnT can be described as a concerted two-electron exchange between **1-core** and **2**: one electron in the π* of **1-core** migrates to the π* orbital of $C_\alpha$=$C_\beta$ double bond in **2** and one electron in the π orbital of $C_\alpha$=$C_\beta$ double bond in **2** moves to the π level of **1-core**. Consequently, the spatial proximity between the π and π* levels of **1-core** and **2** increases the electronic coupling ($V_{TTEnT}$). In the *syn*-conformer, the donor-acceptor orbitals show good spatial overlap, as the $C_\alpha$=$C_\beta$ double bond of **2** aligns with the carbonyl π and π* orbitals of **1-core**. On the contrary, the overlap is weak in the *anti*-conformers as the double bond of **2** and the π and π* orbitals of the carbonyl group of **1-core** are spatially separated (Figure 5a). As a consequence, the *syn*-adducts demonstrate higher electronic couplings than the *anti*-counterparts.

Based on these findings, we propose a novel design principle for photocatalysts that leverages the intrinsic preference in the rate of TTEnT. By restraining the rotation of **1-core** (Figure S3), the photocatalyst will induce an asymmetric activation in favor of the *syn*-adducts, making [2+2] cycloaddition more favorable for the *syn*-adducts over the *anti*-adducts. With the restraint, one may modify the **1-backbone** to facilitate one hydrogen bonding with the substrate while retaining asymmetric induction. In such a case, the substrate may arrange in both *syn*- and *anti*-fashion, yet the *si*-face attack will be facile because the TTEnT process is 100 times faster in the *syn*-adduct compared to the *anti*-adduct due to efficient orbital interaction. Consequently, the cycloaddition in the *syn*-encounter complex will be preferred, leading to enantioselective reactions.

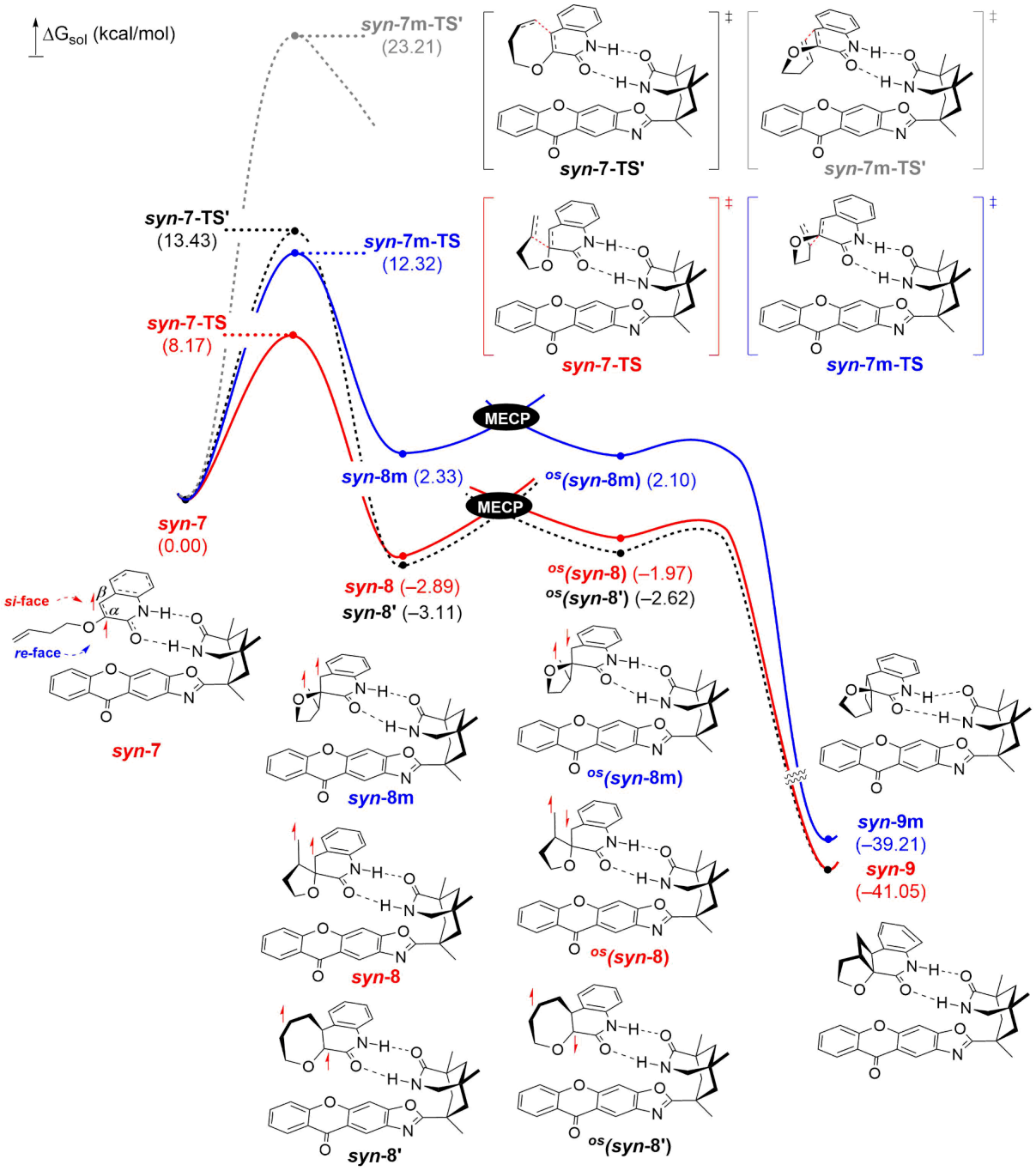


**Figure 6**. Calculated free energy profile for the [2+2] cycloaddition steps

Finally, we delved into the detailed bond-forming steps in the enantioselective [2+2] cycloaddition. Upon completion of the TTEnT, the cyclization process ensues, during which the bond formation events take place, as shown in Figure 6. We optimized the structures of intermediates and the transition states at the UB3LYP-D3/cc-pVTZ(-f)//UB3LYP-D3/6-31G(d,p)/SCRF(ε=9.18) level of the theory, using the lowest-in-energy ***syn-7*** found from the conformer searches. For each located structure,

Gibbs free energy in the solution phase ($\Delta G_{sol}$) was computed, which incorporates the solvation energy, the zero-point energy, and the entropic contributions (See Methods in SI for details). Firstly, we followed the reaction trajectory leading to the major product shown in red. In ***syn-7***, the vinyl moiety approaches the $C_\alpha$=$C_\beta$ double bond on the quinolone ring from the *si*-face, whereas the *re*-face attack is hindered due to the steric constraint imposed by the photosensitizer. Our calculations suggest that the [2+2] cycloaddition occurs in a stepwise manner, forming the two C–C bonds sequentially, in good agreement with previous investigations.[24] The preferred pathway involves bond formation between the internal carbon of the vinyl group and the $C_\alpha$ of the quinolone core, with an activation barrier of 8.2 kcal/mol (***syn*-7-TS**), yielding a five-membered spirocyclic intermediate ***syn*-8**. On the other hand, the coupling between the terminal carbon of the vinyl group and the $C_\beta$ carbon of quinolone was predicted to be notably slower, with a barrier of 13.4 kcal/mol (***syn*-7-TS'**), resulting in a 7-membered ring intermediate, ***syn*-8'**. The lower energy of ***syn*-7-TS** over ***syn*-7-TS'** is attributed to the favorable orbital interaction of the former. As shown in Figure S2, the two pairs of π-antibonding orbitals of the approaching alkenes show in-phase overlaps in ***syn-7-TS***, while only a pair of π-antibonding orbital exhibits favorable interaction in ***syn-7-TS'***. After the formation of the first C–C bond, reverse intersystem crossing (RISC) to the singlet manifold follows to yield the open-shell singlet species, ***$^{os}$(syn-8)*** and ***$^{os}$(syn-8')***. Lastly, the ring-closing step is calculated to be barrierless, leading to the formation of the cyclobutane functionality. This DFT result is in good agreement with CASSCF(6,6)/6-31G* level of calculations that estimated the barriers of similar ring closing processes to be ~1 kcal/mol.[16]

We also followed the pathway of the *re*-face attack, which resulted in the minor product. The computed activation barrier of the first bond-forming step leading to a five-membered ring intermediate ***syn*-8m** is 12.3 kcal/mol (***syn*-7m-TS**), which is 4.1 kcal/mol higher than that of the major product (***syn*-7-TS**). The activation barrier for an eight-membered intermediate was 23.2 kcal/mol (***syn*-7-TS'**), precluding its viability. In short, the comparison of the reaction energy profiles leading to the major and the minor product highlights the role of chiral constrict provided by the hydrogen bonding interaction between the chiral photosensitizer and the substrate.

## Conclusion

In conclusion, the mechanism of [2+2] photocycloaddition of an enone **2** catalyzed by the chiral organic photocatalyst **1** was elucidated. We quantified the rates of ISC and TTEnT steps that produce the activated triplet substrates, which carry out the [2+2] cycloaddition. Owing to the possible rotation of the photoactive **1-core** relative to the hydrogen bonding

scaffold **1-backbone**, various arrangements between **1-core** and substrate **2** are accessible, categorized as *syn*- or *anti-adduct*. The two adducts gave comparable rates for ISC: 1.4 x $10^{11}$ $s^{-1}$ for *syn*-adduct and 6.8 x $10^{10}$ $s^{-1}$ for *anti*-adduct, manifesting the intramolecular nature of the transition within **1-core**. The computed rate of TTEnT in the *syn*-adduct was 3.7 x $10^{12}$ $s^{-1}$, which is ca. 100 times faster than that of the *anti*-adduct (4.0 x $10^{10}$ $s^{-1}$). The strength of electronic coupling is a crucial parameter that explains the difference in the TTEnT rates. For the *syn*-complexes, the computed electronic couplings are linearly dependent on the distance between donor **1-core** and acceptor **2**, while those of the *anti*-complexes did not show a correlation. For the *syn*-complexes, we showed that the orbital overlap between the carbonyl group of **1-core** and $C_\alpha$=$C_\beta$ bond of **2** is maximized, which explains the higher electronic coupling of the isomer over the *anti*-isomer. Overall, our computational investigations manifest the importance of encounter complex geometry in designing the TTEnT-mediated photocatalytic [2+2] cycloaddition reactions.

In addition to providing detailed insights into the xanthone-catalyzed photochemical [2+2] cycloaddition, this work demonstrates the effectiveness of combining Marcus theory and time-dependent DFT in investigating underlying mechanisms of how excited states are accessed and what determines efficient coupling between photocatalyst and substrates. Initially, there were significant reservations about whether these relatively simple and approximate theoretical methods would be capable of capturing the key electronic features of photochemical reactions. Often, much more elaborate and technically more challenging multi-reference ab initio methods are assumed to be necessary - while conceptually more rigorous, these methods come at a disadvantage that results are much more difficult to interpret. The current model allows us to identify concepts that are intuitively understandable and simple, such as donor-acceptor orbital overlaps, that control the observed chemical reactivity.

Moving forward, this technical framework for modeling TTEnT processes can pave the way for additional research. For example, recent reports by the groups of Bach, Weaver, and Gilmore describe photocatalytic deracemization reactions of a racemic mixture of allene[45] and E/Z-olefins.[46–48] These transformations exploit the TTEnT as the key mechanistic step that activates the double bonds, initiating the *cis-trans* isomerization. The modeling framework and analysis methods presented in this work hold the potential to offer insight into the electronic driving forces governing energy transfer and chemical reaction patterns in such photocatalytic processes.

## Author contributions

EL, JP, and MHB conceived the project. EL, HM, and JP carried out the computational modeling of the reaction under the supervision of MHB. EL, HM, JP, and MHB wrote the manuscript.

## Conflicts of interest

There are no conflicts to declare.

## Data availability

All materials supporting the main article are provided in ESI including computational details and Cartesian coordinates of all computed structures.

## Acknowledgments

Authors thank Hoimin Jung for his stimulating discussions for the inception of the project. MHB acknowledges financial support from the Institute for Basic Science (IBS-R10-A1).

## TOC

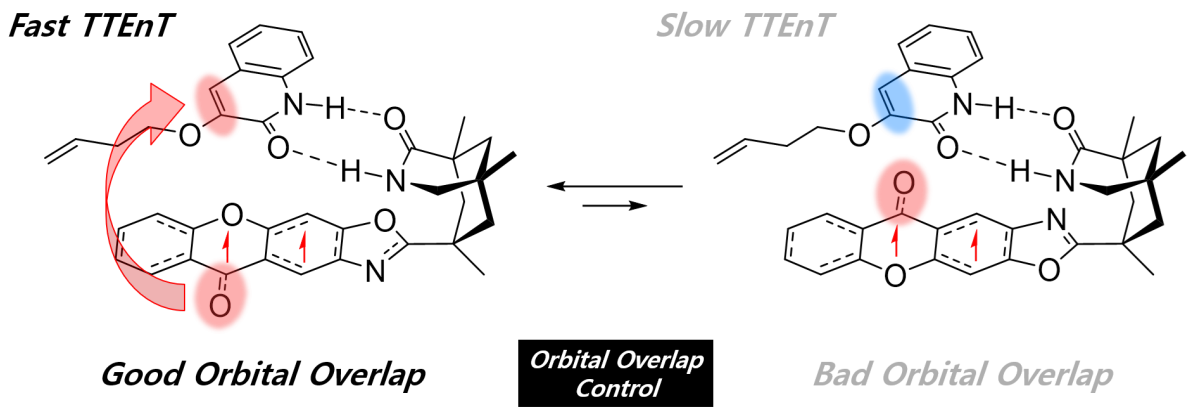


## Reference

(1) Poplata, S.; Tröster, A.; Zou, Y.-Q.; Bach, T. Recent Advances in the Synthesis of Cyclobutanes by Olefin [2 + 2] Photocycloaddition Reactions. *Chem. Rev.* **2016**, *116* (17), 9748–9815.

(2) Müller, C.; Bauer, A.; Bach, T. Light-Driven Enantioselective Organocatalysis. *Angew. Chem. Int. Ed.* **2009**, *48* (36), 6640–6642.
(3) Müller, C.; Bauer, A.; Maturi, M. M.; Cuquerella, M. C.; Miranda, M. A.; Bach, T. Enantioselective Intramolecular [2 + 2]-Photocycloaddition Reactions of 4-Substituted Quinolones Catalyzed by a Chiral Sensitizer with a Hydrogen-Bonding Motif. *J. Am. Chem. Soc.* **2011**, *133* (41), 16689–16697.
(4) Maturi, M. M.; Wenninger, M.; Alonso, R.; Bauer, A.; Pöthig, A.; Riedle, E.; Bach, T. Intramolecular [2+2] Photocycloaddition of 3- and 4-(But-3-Enyl)oxyquinolones: Influence of the Alkene Substitution Pattern, Photophysical Studies, and Enantioselective Catalysis by a Chiral Sensitizer. *Chem. Eur. J.* **2013**, *19* (23), 7461–7472.
(5) Maturi, M. M.; Bach, T. Enantioselective Catalysis of the Intermolecular [2+2] Photocycloaddition between 2-Pyridones and Acetylenedicarboxylates. *Angew. Chem. Int. Ed.* **2014**, *53* (29), 7661–7664.
(6) Alonso, R.; Bach, T. A Chiral Thioxanthone as an Organocatalyst for Enantioselective [2+2] Photocycloaddition Reactions Induced by Visible Light. *Angew. Chem. Int. Ed.* **2014**, *53* (17), 4368–4371.
(7) Tröster, A.; Alonso, R.; Bauer, A.; Bach, T. Enantioselective Intermolecular [2 + 2] Photocycloaddition Reactions of 2(1H)-Quinolones Induced by Visible Light Irradiation. *J. Am. Chem. Soc.* **2016**, *138* (25), 7808–7811.
(8) Vallavoju, N.; Selvakumar, S.; Jockusch, S.; Sibi, M. P.; Sivaguru, J. Enantioselective Organo-Photocatalysis Mediated by Atropisomeric Thiourea Derivatives. *Angew. Chem. Int. Ed.* **2014**, *53* (22), 5604–5608.
(9) Cauble, D. F.; Lynch, V.; Krische, M. J. Studies on the Enantioselective Catalysis of Photochemically Promoted Transformations: “Sensitizing Receptors” as Chiral Catalysts. *J. Org. Chem.* **2003**, *68* (1), 15–21.
(10) Skubi, K. L.; Kidd, J. B.; Jung, H.; Guzei, I. A.; Baik, M.-H.; Yoon, T. P. Enantioselective Excited-State Photoreactions Controlled by a Chiral Hydrogen-Bonding Iridium Sensitizer. *J. Am. Chem. Soc.* **2017**, *139* (47), 17186–17192.
(11) Zheng, J.; Swords, W. B.; Jung, H.; Skubi, K. L.; Kidd, J. B.; Meyer, G. J.; Baik, M.-H.; Yoon, T. P. Enantioselective Intermolecular Excited-State Photoreactions Using a Chiral Ir Triplet Sensitizer: Separating Association from Energy Transfer in Asymmetric Photocatalysis. *J. Am. Chem. Soc.* **2019**, *141* (34), 13625–13634.
(12) Chapman, S. J.; Swords, W. B.; Le, C. M.; Guzei, I. A.; Toste, F. D.; Yoon, T. P. Cooperative Stereoinduction in Asymmetric Photocatalysis. *J. Am. Chem. Soc.* **2022**, *144* (9), 4206–4213.
(13) Corey, E. J.; Bass, J. D.; LeMahieu, R.; Mitra, R. B. A Study of the Photochemical Reactions of 2-Cyclohexenones with Substituted Olefins. *J. Am. Chem. Soc.* **1964**, *86* (24), 5570–5583.
(14) De Mayo, P. Photochemical Syntheses. 37. Enone Photoannelation. *Acc. Chem. Res.* **1971**, *4* (2), 41–47.
(15) Schuster, D. I.; Kaprinidis, N.; Wink, D. J.; Dewan, J. C. Stereochemistry of [2+2] Photocycloaddition of Cyclic Enones to Alkenes: Structural and Mechanistic Considerations in Formation of Trans-Fused Cycloadducts. *J. Org. Chem.* **1991**, *56* (2), 561–567.
(16) Wilsey, S.; González, L.; Robb, M. A.; Houk, K. N. Ground- and Excited-State Surfaces for the [2+2]-Photocycloaddition of α,β-Enones to Alkenes. *J. Am. Chem. Soc.* **2000**, *122* (24), 5866–5876.
(17) Olivucci, M.; Ragazos, I. N.; Bernardi, F.; Robb, M. A. A Conical Intersection Mechanism for the Photochemistry of Butadiene. A MC-SCF Study. *J. Am. Chem. Soc.* **1993**, *115* (9), 3710–3721.
(18) Doubleday, C., Jr. Tetramethylene. *J. Am. Chem. Soc.* **1993**, *115* (25), 11968–11983.
(19) Strieth-Kalthoff, F.; James, M. J.; Teders, M.; Pitzer, L.; Glorius, F. Energy Transfer Catalysis Mediated by Visible Light: Principles, Applications, Directions. *Chem. Soc. Rev.* **2018**, *47* (19), 7190–7202.

(20) Zhou, Q.-Q.; Zou, Y.-Q.; Lu, L.-Q.; Xiao, W.-J. Visible-Light-Induced Organic Photochemical Reactions through Energy-Transfer Pathways. *Angew. Chem. Int. Ed.* **2019**, *58* (6), 1586–1604.
(21) Strieth-Kalthoff, F.; Glorius, F. Triplet Energy Transfer Photocatalysis: Unlocking the Next Level. *Chem* **2020**, *6* (8), 1888–1903.
(22) Dexter, D. L. A Theory of Sensitized Luminescence in Solids. *J. Chem. Phys.* **1953**, *21* (5), 836–850.
(23) Yang, Y.; Wen, Y.; Dang, Z.; Yu, H. Mechanistic Investigation of Visible-Light-Induced Intermolecular [2 + 2] Photocycloaddition Catalyzed with Chiral Thioxanthone. *J. Phys. Chem. A* **2017**, *121* (23), 4552–4559.
(24) Zhou, T.-P.; Zhong, F.; Wu, Y.; Liao, R.-Z. Regioselectivity and Stereoselectivity of Intramolecular [2 + 2] Photocycloaddition Catalyzed by Chiral Thioxanthone: A Quantum Chemical Study. *Org. Biomol. Chem.* **2021**, *19* (7), 1532–1540.
(25) Daub, M. E.; Jung, H.; Lee, B. J.; Won, J.; Baik, M.-H.; Yoon, T. P. Enantioselective [2+2] Cycloadditions of Cinnamate Esters: Generalizing Lewis Acid Catalysis of Triplet Energy Transfer. *J. Am. Chem. Soc.* **2019**, *141* (24), 9543–9547.
(26) Sherbrook, E. M.; Jung, H.; Cho, D.; Baik, M.-H.; Yoon, T. P. Brønsted Acid Catalysis of Photosensitized Cycloadditions. *Chem. Sci.* **2020**, *11* (3), 856–861.
(27) Ma, L.; Fang, W.-H.; Shen, L.; Chen, X. Regulatory Mechanism and Kinetic Assessment of Energy Transfer Catalysis Mediated by Visible Light. *ACS Catal.* **2019**, *9* (4), 3672–3684.
(28) Yang, Y.; Liu, L.; Fang, W.-H.; Shen, L.; Chen, X. Theoretical Exploration of Energy Transfer and Single Electron Transfer Mechanisms to Understand the Generation of Triplet Nitrene and the C(sp3)-H Amidation with Photocatalysts. *JACS Au* **2022**, *2* (11), 2596–2606.
(29) Peng, Q.; Niu, Y.; Shi, Q.; Gao, X.; Shuai, Z. Correlation Function Formalism for Triplet Excited State Decay: Combined Spin-Orbit and Nonadiabatic Couplings. *J. Chem. Theory Comput.* **2013**, *9* (2), 1132–1143.
(30) You, Z.-Q.; Hsu, C.-P.; Fleming, G. R. Triplet-Triplet Energy-Transfer Coupling: Theory and Calculation. *J. Chem. Phys.* **2006**, *124* (4), 044506.
(31) Hsu, C.-P.; You, Z.-Q.; Chen, H.-C. Characterization of the Short-Range Couplings in Excitation Energy Transfer. *J. Phys. Chem. C* **2008**, *112* (4), 1204–1212.
(32) Kasha, M. Characterization of Electronic Transitions in Complex Molecules. *Discuss. Faraday Soc.* **1950**, *9* (0), 14–19.
(33) Zhang, Z.; Yi, D.; Zhang, M.; Wei, J.; Lu, J.; Yang, L.; Wang, J.; Hao, N.; Pan, X.; Zhang, S.; Wei, S.; Fu, Q. Photocatalytic Intramolecular [2 + 2] Cycloaddition of Indole Derivatives via Energy Transfer: A Method for Late-Stage Skeletal Transformation. *ACS Catal.* **2020**, *10* (17), 10149–10156.
(34) Ha, S.; Lee, Y.; Kwak, Y.; Mishra, A.; Yu, E.; Ryou, B.; Park, C.-M. Alkyne-Alkene [2 + 2] Cycloaddition Based on Visible Light Photocatalysis. *Nat. Commun.* **2020**, *11* (1), 2509.
(35) Arai, N. Intramolecular [2 + 2] Cycloaddition of Isocarbostyrils Catalyzed by an Iridium Visible-Light Photocatalyst. *J. Org. Chem.* **2023**, *88* (7), 4848–4853.
(36) Based on Transition-State Theory of Adiabatic Reaction and the Eyring Equation, the Rate and Activation Energy Barrier Are Correlated by the Equation: K =(kbT/h)exp(ΔG‡/RT), Where K Is the Rate Constant, Kb Is the Boltzmann Constant, H Is the Plank constant,ΔG‡ Is the Energetic Barrier of Activation, R Is the Gas Constant, and T Is Temperature.
(37) Cavaleri, J. J.; Prater, K.; Bowman, R. M. An Investigation of the Solvent Dependence on the Ultrafast Intersystem Crossing Kinetics of Xanthone. *Chem. Phys. Lett.* **1996**, *259* (5), 495–502.
(38) Baba, M.; Kamei, T.; Kiritani, M.; Yamauchi, S.; Hirota, N. A Phosphorescence Study of Jet-Cooled Xanthone. *Chem. Phys. Lett.* **1991**, *185* (3), 354–358.
(39) Ohshima, Y.; Fujii, T.; Fujita, T.; Inaba, D.; Baba, M. S1 1A2(nπ*) and S2 1A1(ππ*) States of Jet-Cooled Xanthone. *J. Phys. Chem. A* **2003**, *107* (42), 8851–8855.
(40) Satzger, H.; Schmidt, B.; Root, C.; Zinth, W.; Fierz, B.; Krieger, F.; Kiefhaber, T.; Gilch, P.

Ultrafast Quenching of the Xanthone Triplet by Energy Transfer: New Insight into the Intersystem Crossing Kinetics. *J. Phys. Chem. A* **2004**, *108* (46), 10072–10079.
(41) Heinz, B.; Schmidt, B.; Root, C.; Satzger, H.; Milota, F.; Fierz, B.; Kiefhaber, T.; Zinth, W.; Gilch, P. On the Unusual Fluorescence Properties of Xanthone in Water. *Phys. Chem. Chem. Phys.* **2006**, *8* (29), 3432–3439.
(42) Alías-Rodríguez, M.; de Graaf, C.; Huix-Rotllant, M. Ultrafast Intersystem Crossing in Xanthone from Wavepacket Dynamics. *J. Am. Chem. Soc.* **2021**, *143* (51), 21474–21477.
(43) Vura-Weis, J.; Abdelwahed, S. H.; Shukla, R.; Rathore, R.; Ratner, M. A.; Wasielewski, M. R. Crossover from Single-Step Tunneling to Multistep Hopping for Molecular Triplet Energy Transfer. *Science* **2010**, *328* (5985), 1547–1550.
(44) Voityuk, A. A. Triplet Excitation Energy Transfer through Fluorene π Stack. *J. Phys. Chem. C* **2010**, *114* (47), 20236–20239.
(45) Hölzl-Hobmeier, A.; Bauer, A.; Silva, A. V.; Huber, S. M.; Bannwarth, C.; Bach, T. Catalytic Deracemization of Chiral Allenes by Sensitized Excitation with Visible Light. *Nature* **2018**, *564* (7735), 240–243.
(46) Neveselý, T.; Molloy, J. J.; McLaughlin, C.; Brüss, L.; Daniliuc, C. G.; Gilmour, R. Leveraging the N→π* Interaction in Alkene Isomerization by Selective Energy Transfer Catalysis. *Angew. Chem. Int. Ed.* **2022**, *61* (2), e202113600.
(47) Singh, K.; Staig, S. J.; Weaver, J. D. Facile Synthesis of Z-Alkenes via Uphill Catalysis. *J. Am. Chem. Soc.* **2014**, *136* (14), 5275–5278.
(48) Metternich, J. B.; Gilmour, R. A Bio-Inspired, Catalytic E → Z Isomerization of Activated Olefins. *J. Am. Chem. Soc.* **2015**, *137* (35), 11254–11257.